The Astrophysical Journal, 945:64 (5pp), 2023 March 1 https://doi.org/10.3847/1538-4357/acb93c

First Analysis of In Situ Observation of Surface Alfvén Waves in an ICME Flux Rope

Anil Raghav[1], Omkar Dhamane[1], Zubair Shaikh[2], Naba Azmi[1], Ankita Manjrekar[1,2], Utsav Panchal[1], Kalpesh Ghag[1], Daniele Telloni[3], Raffaella D'Amicis[4], Prathmesh Tari[1], and Akshata Gurav[1]
[1] Department of Physics, University of Mumbai, Mumbai, India; raghavanil1984@gmail.com
[2] Indian Institute of Geomagnetism, Panvel, Navi Mumbai, India
[3] National Institute for Astrophysics, Astrophysical Observatory of Torino, Via Osservatorio 20, I-10025 Pino Torinese, Italy; daniele.telloni@inaf.it
[4] National Institute for Astrophysics, Institute for Space Astrophysics and Planetology, Via del Fosso del Cavaliere 100, I-00133 Roma, Italy
Received 2022 November 29; revised 2023 February 2; accepted 2023 February 2; published 2023 March 7

Abstract

Alfvén waves (AWs) are ubiquitous in space and astrophysical plasma. Their crucial role in various physical processes has triggered intense research in solar–terrestrial physics. Simulation studies have proposed the generation of AWs along the surface of a cylindrical flux rope, referred to as surface AWs (SAWs); however, the observational verification of this distinct wave has been elusive to date. We report the first in situ observation of SAWs in a flux rope of an interplanetary coronal mass ejection. We apply the Walén test to identify them. We have used Elsässer variables to estimate the characteristics of SAWs. They may be excited by the movement of the flux rope's footpoints or by instabilities along the boundaries of the plasma magnetic cloud. Here, the change in plasma density or field strength in the surface-aligned magnetic field may trigger SAWs.

Unified Astronomy Thesaurus concepts: Alfven waves (23); Space plasmas (1544); Solar coronal mass ejections (310)

1. Introduction

Magnetohydrodynamic Alfvén waves (AWs) are ubiquitous plasma wave modes in space and astrophysical regimes. In these waves, ions collectively respond to perturbations in the ambient magnetic field, such that the ions provide inertia, while the magnetic field supplies the required restoring force (Alfvén 1942). The fluid velocity and magnetic field fluctuations propagating in the direction of the magnetic tension force, i.e., well-correlated changes in the respective components of the magnetic field and plasma velocity, lead to the apparent characterization of AWs (Walén 1944; Hudson 1971; Yang & Chao 2013; Raghav & Kule 2018a). In heliospheric plasma, AWs are observed in two forms: arc-polarized Alfvén waves that have often been recognized in the solar wind (Belcher & Davis 1971; Wang et al. 2012) and tube modes in ideal magnetic flux ropes, such as the torsional mode (Gosling et al. 2010; Raghav et al. 2018). These modes are appealing because they carry significant energy from the subphotospheric regions to the corona, and provide energy for coronal heating (Van Doorsselaere et al. 2008). There is a high possibility of identifying AWs in interplanetary space when a magnetic flux rope erupts, no matter the mode in which they are present (Wang et al. 2019), However, sometimes they are hardly distinguishable from a flux rope configuration (Higginson & Lynch 2018), and therefore their interrelationships are more complex than reported in several studies.

It is worth noting that a coronal mass ejection (CME) is an eruption of enormous energy and massive magnetized plasma from the solar corona into the heliosphere in the form of a magnetic flux rope (Howard 2011; Webb & Howard 2012). Magnetic reconnection or catastrophic processes are expected to trigger low-frequency AWs and fast- and slow-mode magnetoacoustic waves during the initiation of a CME (Kopp & Pneuman 1976). Thus, the Sun is considered a significant source of outward AWs (Belcher & Davis 1971). Moreover, the reported inward AWs suggest different generation mechanisms apart from the ones mentioned above. Inward AWs are observed in (1) regions of back-streaming ions from the Earth's bow shock (He et al. 2015), and (2) regions immediately upstream and downstream of reverse shocks associated with corotating interaction regions or the interplanetary counterparts of CMEs (ICMEs; Tsurutani et al. 2009). AWs are also found in the vicinity of reconnection exhausts and during the drifting of sunward proton beams in the solar wind (Belcher & Davis 1971; Roberts et al. 1987; Bavassano & Bruno 1989; Gosling et al. 2009, 2011). It is also proposed that they may be triggered by some physical processes happening locally (Bavassano et al. 2001; Bruno & Carbone 2013). Recently, we found their existence during CME–CME and CME–HSS interactions, and inside the ICME sheath regions (Raghav & Kule 2018a, 2018b; Dhamane et al. 2022; Raghav et al. 2022). Moreover, AWs play a key role in modulating the recovery phase of geomagnetic storms and slowing down the restoration of the magnetosphere toward its pre-storm equilibrium state (Raghav et al. 2018, 2019; Shaikh et al. 2019b; Choraghe et al. 2021; Telloni et al. 2021).

The most interesting MHD surface wave in the astrophysical domain is the surface Alfvén wave (SAW). It forms when there is a boundary of finite thickness between two regions of plasma with substantial inhomogeneity in a magnetic field and/or in density (Evans et al. 2009). SAWs may propagate through surface and filamentary structures (e.g., discontinuities) in interplanetary and interstellar space (Wentzel 1979). Their coupling with kinetic Alfvén waves dissipates them and heats up the surface (Chen & Hasegawa 1974; Hasegawa & Chen 1976). Moreover, Wentzel (1979) suggested that SAWs may be triggered by movement of the footpoints of flux tubes or by instabilities along the plasma boundaries. Theory and experiment suggest that the SAW eigenmodes play a crucial

role in the heating process of AWs (Amagishi 1986; Ruderman & Goossens 1996). A simulation studying the collision between a shock wave and a magnetic flux tube shows that SAWs can be generated and propagated along the flux tube (Sakai et al. 2000). It further suggests that SAWs are possible for magnetic flux tubes with weak electric current, whereas body AWs may be generated when the current is strong. Moreover, Lehane & Paoloni (1972) confirmed SAWs in the laboratory.

Alfvén (1942) investigated the properties of plasma, assuming the plasma medium to be a highly conducting, magnetized, and incompressible fluid. He found that a distinctive wave mode arises in the fluid, which propagates in the magnetic field direction and is known as a shear or torsional Alfvén wave (Cramer 2011). It propagates energy through the medium's intrinsic elastic and tensile characteristics. SAWs are a second class of waves that are supported by the presence of nonuniformities, such as variations in the Alfvén speed. They become more significant as the scale length of the nonuniformity diminishes (Ionson 1978). Unlike ordinary hydromagnetic body waves, SAWs are supported by the elasticity afforded by nonuniformities. In the solar wind, surface waves can do work on the expanding gas of the wind much as ordinary body hydromagnetic waves do (Hollweg 1975). In an infinite uniform plasma, Alfvén waves are driven solely by the magnetic tension force and they are the only waves that propagate vorticity. The displacements are vortical and incompressible. Goossens et al. (2012) investigated the modification of MHD waves in the presence of a nonuniform density and/or magnetic field. They found that incompressible SAWs have vorticity equal to zero everywhere except at the discontinuity, where all vorticity is concentrated. Thus, the behavior of SAWs is clearly different from that of classic Alfvén waves.

Theory and simulation studies suggest the existence of SAWs in magnetic flux rope structures, but observational evidence has yet to be found in either small- or large-scale (like the ICME) flux ropes. Here, we investigated 401 ICME events listed in the catalog of Earth-directed ICMEs measured by the WIND spacecraft and we hunted for in situ evidence of SAWs. Interestingly, we found three potential events for SAWs. The best of these events is discussed here in detail. To the best of our knowledge, this is the first observational report of SAWs superposed on an ICME flux rope.

2. Data and Method

The ICME flux rope event was identified on 2005 September 2 by the WIND spacecraft. We have used magnetic field and plasma data (of 3 s time resolution) from the Magnetic Field Investigation (MFI; Lepping et al. 1995) and the 3DP Solar Wind Experiment (SWE; Ogilvie et al. 1995) instruments on board the WIND spacecraft in geocentric solar ecliptic coordinates. Their variation with 92 s time resolution during the studied event is demonstrated in Figure 1. The sudden increase in the total magnetic field $B_{\rm tot}$, number density (N_p), total pressure ($P_{\rm tot}$), and plasma temperature (T_p) indicates the onset of the shock front. The Rankine–Hugoniot relation confirms the presence of the shock. The details are available at CfA Interplanetary Shock Database.[5] Large fluctuations are observed in each magnetic field component, and the following

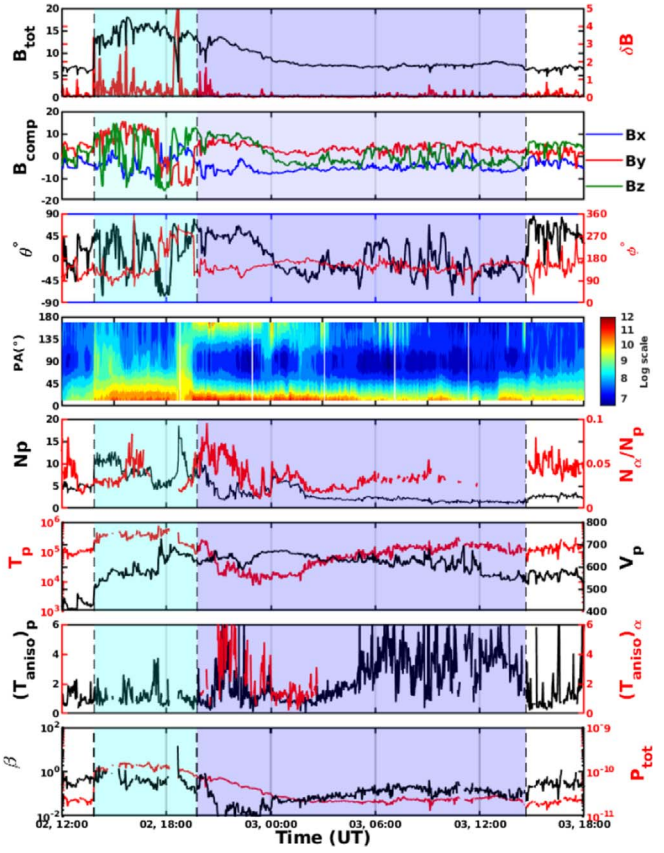

Figure 1. Plot of the WIND data over the interval 2005 September 2 12:00:00 to 2005 September 3 18:00:00 UT. From top to bottom: interplanetary magnetic field (IMF) strength $B_{\rm tot}$ overlaid with δB, a component of the magnetic field $B_{\rm comp}$, the IMF orientation of θ and ϕ, the pitch angle (PA) of suprathermal electron strahls, the variation of number density N_p and N_α/N_p. the variation of temperature (T_p) and velocity (V_p) of protons, the anisotropy in proton temperature $(T_{\rm aniso})_p$ and α-particle temperature $(T_{\rm aniso})_\alpha$, and the plasma β overlaid with plasma thermal pressure $P_{\rm tot}$.

region is generally referred to as the ICME sheath region (see the cyan shaded interval). We observe a value near 1 for β along with high proton density, high plasma temperature, and an enhanced solar wind speed in this region. The ICME flux rope follows the sheath region (see the blue shaded region). The ICME flux rope shows a gradual decrease in total magnetic field, a decrease in the fluctuations in magnetic field components, a low plasma temperature, and low plasma β value. Moreover, during flux rope transit, we observed a nearly bidirectional flow of electrons from the variation in electron pitch angle. The different boundaries are defined in two distinct catalogs available online, i.e., the Richardson/Cane catalog of ICMEs[6] and the USTC ICME catalog.[7]

To identify Alfvén waves, we have employed the Walén relation described as (Walén 1949; Hudson 1971)

$$\Delta V = |R_{\rm W}|\,\Delta V_{\rm A}.$$

Here, the linear relation between fluctuations in Alfvén velocity ($\Delta V_{\rm A} = \Delta B/\sqrt{\rho_p \mu_0}$) and solar wind velocity (ΔV) provides the Walén slope ($R_{\rm W}$). The fluctuations in the magnetic field ΔB and proton flow velocity ΔV are determined by removing the background field value (B_0) from measured

[5] http://www.cfa.harvard.edu/shocks/wi_data/00530/wi_00530.html

[6] http://www.srl.caltech.edu/ACE/ASC/DATA/level3/icmetable2.htm

[7] http://space.ustc.edu.cn/dreams/wind_icmes

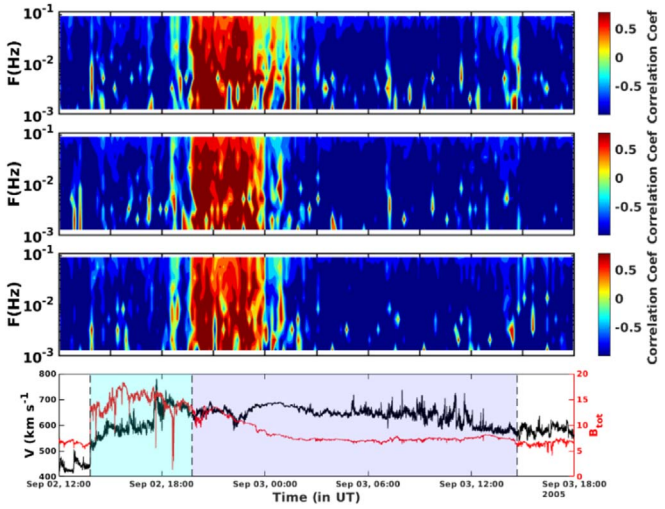

Figure 2. The time–frequency domain gives the correlation coefficient between V_{Ai} and V_i for the entire event. The bottom panel displays the changes in the magnetic field and proton velocity over time. The vertical dashed line shows the boundaries of the (magnetic cloud) MC and shock sheath of the ICME. For the above analysis, we use 3 s data from the WIND spacecraft.

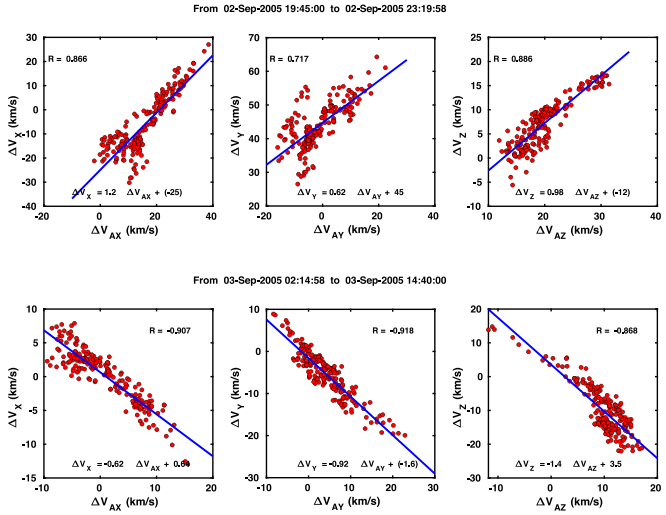

Figure 3. Analysis of the correlation between corresponding ΔV and ΔV_A components. The red circles represent observations by the WIND spacecraft with a time cadence of 3 s. The coefficient of correlation is denoted by R. Each panel's equation represents a linear relation fitted between the respective components of ΔV and ΔV_A.

values. The significant correlation between the respective components of ΔV_A and ΔV indicates the presence of an Alfvén wave. Determining the background value of V_A and V is challenging while implementing the Walén relation. Reported studies have either used the average values of V_A, and V of the studied duration, or the values derived in the de Hoffmann–Teller frame (HT; Gosling et al. 2010; Yang & Chao 2013; Raghav & Kule 2018a; Raghav et al. 2018; Shaikh et al. 2019a). Here, we used a MATLAB-based algorithm involving the fourth-order Butterworth bandpass filter to estimate background values. Ten evenly divided logarithmic frequency bands were selected. The selected bandpass periods are 10–15 s, 15–25 s, 25–40 s, 40–60 s, 60–100 s, 100–160 s, 160–250 s, 250–400 s, 400–630 s, and 630–1000 s. The complete data under examination are split into windows of 200 data points, i.e., a 10 minute time window. For every window and filtered band, we find the correlation coefficient between the respective components of V_A and V. Figure 2 shows a contour plot of V_{Ai} and V_i along with the temporal variations of total magnetic field and velocity. The sheath and trailing edge of the magnetic cloud (MC) indicate a strong negative correlation coefficient (dark blue shade). This confirms that these regions are superposed on the antisunward flow of AWs. The leading part of the MC exhibits a strong positive correlation coefficient (red shade), confirming the sunward propagation of AWs.

To support our findings, we estimate correlation coefficients between ΔV and ΔV_A for the front and rear parts of the MC, which are shown in Figure 3. We used the fourth-order Butterworth MATLAB filter algorithm with a single broadband frequency boundary of 10^{-3}–10^{-1} Hz to filter the ΔV data and ΔV_A components. The Pearson correlation coefficients (R) for each x, y, and z component for the ICME (MC from 2005 September 2 19:45:00 to 2005 September 2 23:19:58) are 0.866, 0.717, and 0.886, respectively. The strong positive correlation confirmed the sunward nature of the Alfvén waves present in the aforesaid region. Similarly for 2005 September 3 02:14:58 to 2005 September 3 14:40:00 we found R for each x, y, and z component as −0.907, −0.918, and −0.868,

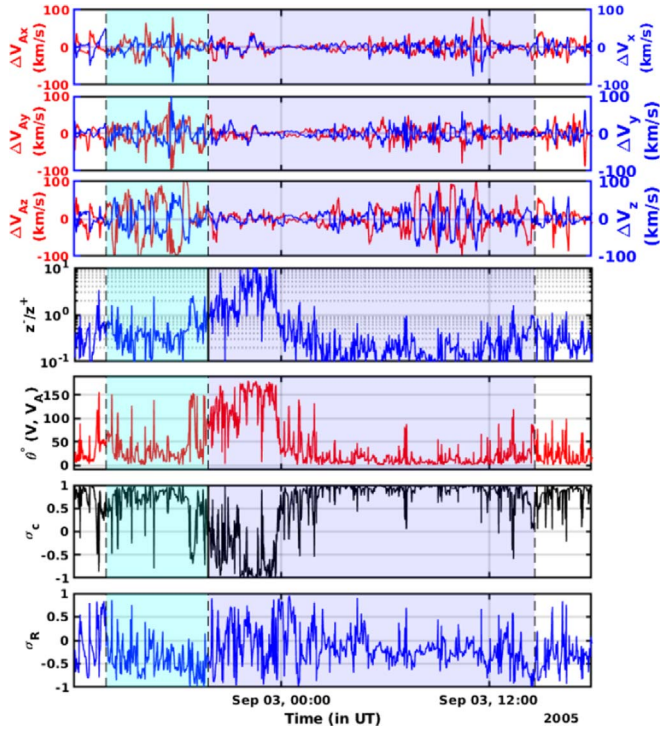

Figure 4. The top three panels show the temporal variation of fluctuations in Alfvén velocity ΔV_{Ai} (red) with fluctuations in proton flow velocity ΔV_i (blue). The ratio of Elsässer variables z^-/z^+ is shown in the fourth panel. The presence of the angle between the magnetic field and solar wind speed is shown in the fifth panel. The last two panels represent the temporal variation of the normalized cross helicity (σ_c) and normalized residual energy (σ_R).

respectively. This negative correlation implies the presence of strong antisunward Alfvén waves.

Figure 4 depicts the plasma properties in the ICME's shock sheath and MC region based on Elsässer variables. The top three panels of Figure 4 show the fluctuations in the components of Alfvénic velocity (ΔV_A) and proton flow velocity (ΔV_p). The fluctuations in each component are obtained by passing each measured component through a

fourth-order Butterworth filter (with frequency limits of 10^{-3}–10^{-1} Hz) algorithm of MATLAB software. We observed anticorrelated flow fluctuations in the sheath region for each component. Interestingly, we found correlated flow fluctuations in the initial part of the MC but anticorrelated flow in its trailing part. Here, we employ Elsässer variables to separate the contributions of outward and inward flows of Alfvénic fluctuations. The Elsässer variables are defined as (Elsasser 1950; Dobrowolny et al. 1980; Marsch & Mangeney 1987; Zhou & Matthaeus 1989)

$$z^{\pm} = \Delta \boldsymbol{V} \pm \frac{\Delta \boldsymbol{B}}{\sqrt{4\pi\rho}} = \Delta \boldsymbol{V} \pm \Delta \boldsymbol{V}_{\rm A}. \quad (1)$$

Here, Elsässer variables z^+ and z^- are set up to find the direction of flow of the waves, i.e., outward and inward, respectively (Roberts et al. 1987). The $\pm$ sign in front of $\boldsymbol{B}$ depends on the sign of $[-k \cdot B_0]$. We observe that, for the ratio $z^-/z^+ < 1$ the outward flow became more effective in the sheath region and the trailing part of the MC, whereas for the ratio >1 the inward Alfvénic fluctuations are dominant in the initial part of the MC (Matthaeus & Goldstein 1982; Tu et al. 1989). The angle between Alfvén velocity and solar wind velocity $\theta(V, V_{\rm A})$ is estimated as

$$\theta(\Delta V_{\rm A}, \Delta V) = \arccos\left(\frac{\Delta \boldsymbol{V}_{\rm A} \cdot \Delta \boldsymbol{V}}{||\Delta \boldsymbol{V}_{\rm A}||\,||\Delta \boldsymbol{V}||}\right).$$

At the beginning of the MC, the two vectors are almost antiparallel to each other, while in the sheath region and trailing part of the MC, the flow is concurrent. This strongly suggests that the flow direction changes in each region.

The cross helicity (H_c) is a measure of the correlation between velocity and magnetic field (Bruno & Carbone 2013). The dimensionless measure of cross helicity is known as normalized cross helicity ($\sigma_c = H_c/E$) and ranges from -1 to 1. For $\sigma_c = \pm 1$, the fluctuations are highly Alfvénic:

$$\sigma_c = \frac{e^+ - e^-}{e^+ + e^-}. \quad (2)$$

Here e^- and e^+ are the energies related to z^- and z^+ and $e^{\pm} = \frac{1}{2}(z^{\pm})^2$. Also, the normalized residual energy is calculated as (Bruno et al. 2005; Bruno & Carbone 2013)

$$\sigma_R = \frac{e^v - e^b}{e^v + e^b}, \quad (3)$$

where e^v and e^b are kinetic and magnetic energy respectively. We observe $\sigma_c > 0$ and $\sigma_R < 0$ in the sheath region and trailing part of the MC (outward). Also, $\sigma_c < 0$ and $\sigma_R > 0$ in the leading part of the MC (inward). These observations strongly agree with the estimation of Elsässer variables.

The intensity of inward/outward propagating waves or their mixing is investigated by using the temporal variations of Walén slope (or the correlation between the magnetic field and plasma velocity; Belcher & Davis 1971; Marsch & Tu 1993; Bruno & Carbone 2013; Yang et al. 2016; Shiota et al. 2017). The temporal fluctuations are depicted in Figure 5. Both coefficients fluctuate near the value of -1 in the sheath region and the trailing part of the MC, whereas they fluctuate around 1 in the leading part of the MC.

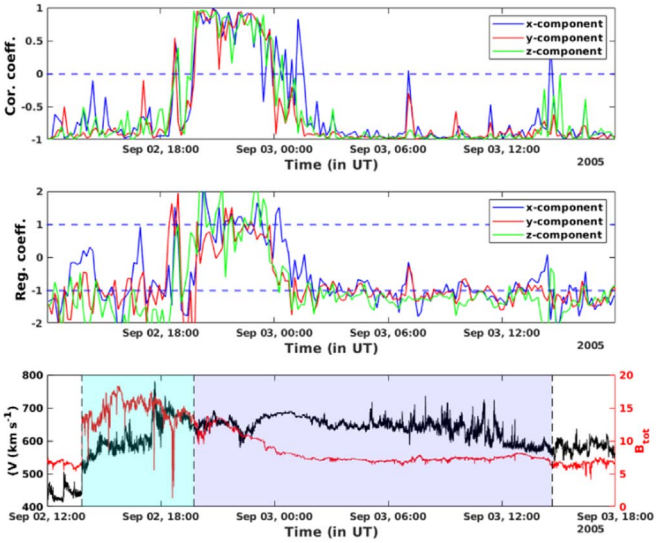

Figure 5. The correlation and regression coefficients are shown in the top two panels, while the variations of total magnetic field ($B_{\rm tot}$) and the solar wind speed (V) with time are shown in the bottom panel.

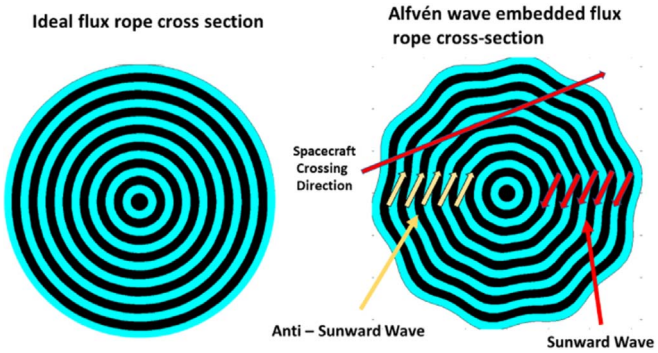

Figure 6. Cartoon depiction of the generation of a SAW: the first image shows the ideal flux rope cross section and the second manifests the spacecraft crossing a cross section of the flux rope.

3. Discussion and Conclusion

All the observations and estimations suggest an outward flow of Alfvén fluctuations in the sheath region, an inward flow in the front part of the MC, and an outward flow in its rear part. This implies two possibilities for AW generation: (i) the interaction between the sheath and MC triggers an oppositely directed wave flow in the sheath region and MC or (ii) the change in the axial current induces Alfvénic fluctuations in the magnetic flux rope. The simulation study corroborates that the collision between a shock wave and a magnetic flux tube describes the generation of SAWs, or the possibilities of SAWs for magnetic flux tubes with weak electric current (Sakai et al. 2000).

As an analogy, the bidirectional flow of an Alfvén wave in the ICME flux rope can be explained as follows. Consider the cartoon picture of the cross section of the flux rope shown in Figure 6. The left image is the ideal circular cross section of the flux rope, whereas the right image shows the cross section of the SAW's superposed flux rope. The red arrow indicates the spacecraft's passage through the ICME flux rope. At the spacecraft's entry point, i.e., the anterior of the flux rope, the surface wave exhibits an upward direction of propagation, whereas the posterior shows downward propagation. The upward and downward directions are proxies for wave propagation. An important fact is that the wave

propagates inward in the initial part of the MC and outward in its trailing region (see Figure 2). When the spacecraft moves from one end of the flux rope's cross section to the other, the amplitude of fluctuations on the surface is more significant than at the center. The outer layer of the flux rope has a greater amplitude of the Alfvénic oscillations. As we move into the inner concentric layers, the amplitude decreases and is minimum at the center of the flux rope. This is also clearly seen in the top three panels of Figure 4.

SAWs are expected to exist in astrophysical plasmas where jumps in density or magnetic field occur, e.g., on the surfaces of magnetic flux tubes in the solar and stellar atmospheres, and at the interfaces between plasmas of different properties in the solar wind and Earth's magnetosphere (Cramer 2011). We also observed a large anisotropy in proton temperature in the front and trailing parts of the flux rope, which could be a possible source of SAW generation or vice versa. Besides this, we observed a spike in number density (N_p) and a sudden drop in the total interplanetary magnetic field (IMF) strength in the sheath region, just prior to the onset of the MC (see Figure 1), which could be attributed to reconnection exhaust. Moreover, Gosling et al. (2005) claims that AWs could be generated by reconnection exhaust at the quasi-stationary heliospheric current sheet, implying that the difference in density variations at the boundary between the sheath region and the MC leads to the induction of oppositely directed waves in the sheath region and the MC's front part.

An AW is often observed in interplanetary space, and most recently has been seen in flux ropes (Gosling et al. 2010; Raghav & Kule 2018b). The behavior of an SAW is entirely different from that of a classical AW (Goossens et al. 2012). SAWs are linked to the tearing mode instability, which leads to time-dependent magnetic reconnection. This results in the neutral collision effect and causes the ionization fraction to significantly impact the SAWs (Uberoi 1994; Uberoi et al. 1996). The resonant absorption of SAWs appears to be a viable heating process for both open regions and coronal loops (Ionson 1978). Moreover, SAWs can damp through viscosity, resistivity, and other kinetic factors, which results in plasma wave heating (Evans et al. 2012). Evans et al. (2009) explored the role of damping by SAWs in solar wind heating. Here, a number of intriguing scientific questions arise, such as: How does a SAW alter the properties of the ICME? How do SAWs dissipate? Additionally, how does the SAW amplitude change as the ICME moves across the heliosphere? These issues are beyond the scope of this article, although we might look into them in the future.

The authors thank Greg Hilbert for valuable suggestions. The authors thank everyone involved in development of the WIND spacecraft mission, including the data-providing team. We also appreciate NASA/Space GSFC's Physics Data Facilities (CDAWeb or ftp) service. SERB, India, is acknowledged since A.R. and O.D. are supported by SERB project reference file CRG/2020/002314. Z.S. also thanks the government of India's "The Department of Science and Technology (DST)" (https://dst.gov.in/) for their cooperation.

ORCID iDs

Anil Raghav https://orcid.org/0000-0002-4704-6706
Omkar Dhamane https://orcid.org/0000-0002-4862-4141
Zubair Shaikh https://orcid.org/0000-0002-9206-6327
Kalpesh Ghag https://orcid.org/0000-0002-9506-6875
Daniele Telloni https://orcid.org/0000-0002-6710-8142
Raffaella D'Amicis https://orcid.org/0000-0003-2647-117X

References

Alfvén, H. 1942, Natur, 150, 405
Amagishi, Y. 1986, PhRvL, 57, 2807
Bavassano, B., & Bruno, R. 1989, JGR, 94, 168
Bavassano, B., Pietropaolo, E., & Bruno, R. 2001, JGR, 106, 10659
Belcher, J. W., & Davis, L. 1971, JGR, 76, 3534
Bruno, R., & Carbone, V. 2013, LRSP, 10, 2
Bruno, R., Carbone, V., Bavassano, B., & Sorriso-Valvo, L. 2005, AdSpR, 35, 939
Chen, L., & Hasegawa, A. 1974, JGR, 79, 1024
Choraghe, K., Raghav, A., Chakrabarty, D., Kasthurirangan, S., & Bijewar, N. 2021, JGRA, 126, e2020JA028685
Cramer, N. F. 2011, The Physics of Alfvén Waves (New York: Wiley)
Dhamane, O., Raghav, A., Shaikh, Z., et al. 2022, arXiv:2209.04682
Dobrowolny, M., Mangeney, A., & Veltri, P. 1980, PhRvL, 45, 144
Elsasser, W. M. 1950, PhRv, 79, 183
Evans, R. M., Opher, M., Jatenco-Pereira, V., & Gombosi, T. I. 2009, ApJ, 703, 179
Evans, R. M., Opher, M., Oran, R., et al. 2012, ApJ, 756, 155
Goossens, M., Andries, J., Soler, R., et al. 2012, ApJ, 753, 111
Gosling, J. T., McComas, D. J., Roberts, D. A., & Skoug, R. M. 2009, ApJL, 695, L213
Gosling, J., Skoug, R., McComas, D., & Smith, C. 2005, JGRA, 110, 101107
Gosling, J. T., Teh, W.-L., & Eriksson, S. 2010, ApJL, 719, L36
Gosling, J. T., Tian, H., & Phan, T. D. 2011, ApJL, 737, L35
Hasegawa, A., & Chen, L. 1976, PhFl, 19, 1924
He, J., Pei, Z., Wang, L., et al. 2015, ApJ, 805, 176
Higginson, A. K., & Lynch, B. J. 2018, ApJ, 859, 6
Hollweg, J. V. 1975, RvGeo, 13, 263
Howard, T. 2011, Coronal Mass Ejections: An Introduction, Vol. 376 (Berlin: Springer)
Hudson, P. D. 1971, P&SS, 19, 1693
Ionson, J. A. 1978, ApJ, 226, 650
Kopp, R. A., & Pneuman, G. W. 1976, SoPh, 50, 85
Lehane, J. A., & Paoloni, F. J. 1972, PlPh, 14, 701
Lepping, R. P., Acũna, M. H., Burlaga, L. F., et al. 1995, SSRv, 71, 207
Marsch, E., & Mangeney, A. 1987, JGR, 92, 7363
Marsch, E., & Tu, C.-Y. 1993, JGR, 98, 21045
Matthaeus, W. H., & Goldstein, M. L. 1982, JGR, 87, 10347
Ogilvie, K. W., Chornay, D. J., Fritzenreiter, R. J., et al. 1995, SSRv, 71, 55
Raghav, A., Shaikh, Z., Dhamane, O., et al. 2022, arXiv:2209.05037
Raghav, A. N., Choraghe, K., & Shaikh, Z. I. 2019, MNRAS, 488, 910
Raghav, A. N., & Kule, A. 2018a, MNRAS, 476, L6
Raghav, A. N., & Kule, A. 2018b, MNRAS, 480, L6
Raghav, A. N., Kule, A., Bhaskar, A., et al. 2018, ApJ, 860, 26
Roberts, D. A., Goldstein, M. L., Klein, L. W., & Matthaeus, W. H. 1987, JGR, 92, 12023
Ruderman, M. S., & Goossens, M. 1996, JPlPh, 56, 107
Sakai, J. I., Kawata, T., Yoshida, K., Furusawa, K., & Cramer, N. F. 2000, ApJ, 537, 1063
Shaikh, Z. I., Raghav, A., & Vichare, G. 2019a, MNRAS, 490, 1638
Shaikh, Z. I., Raghav, A., Vichare, G., et al. 2019b, MNRAS, 490, 3440
Shiota, D., Zank, G. P., Adhikari, L., et al. 2017, ApJ, 837, 75
Telloni, D., D'Amicis, R., Bruno, R., et al. 2021, ApJ, 916, 64
Tsurutani, B. T., Guarnieri, F. L., Echer, E., Lakhina, G. S., & Verkhoglyadova, O. P. 2009, JGRA, 114, A08105
Tu, C.-Y., Marsch, E., & Thieme, K. M. 1989, JGR, 94, 11739
Uberoi, C. 1994, JPlPh, 52, 215
Uberoi, C., Lanzerotti, L. J., & Wolfe, A. 1996, JGR, 101, 24979
Van Doorsselaere, T., Nakariakov, V. M., & Verwichte, E. 2008, ApJL, 676, L73
Walén, C. 1944, ArMAF, 30, 1
Walén, C. 1949, On the Vibratory Rotation of the Sun (Stockholm: Univ. Stockholm)
Wang, X., He, J., Tu, C., et al. 2012, ApJ, 746, 147
Wang, Z., Feng, X., & Zheng, J. 2019, ApJL, 887, L18
Webb, D. F., & Howard, T. A. 2012, LRSP, 9, 2
Wentzel, D. G. 1979, ApJ, 227, 319
Yang, L., & Chao, J. 2013, ChJSS, 33, 353
Yang, L., Lee, L. C., Chao, J. K., et al. 2016, ApJ, 817, 178
Zhou, Y., & Matthaeus, W. H. 1989, GRL, 16, 755